Biophysical Journal, Volume *114*

Supplemental Information

FRET Detects the Size of Nanodomains for Coexisting Liquid-Disordered and Liquid-Ordered Phases

Thais A. Enoki, Frederick A. Heberle, and Gerald W. Feigenson

FRET detects the size of nanodomains for coexisting liquid-disordered + liquid-ordered phases

T. A. Enoki, F. A. Heberle and G. W. Feigenson

Contents

1 Phase diagrams and fraction of phases along the tieline

Well-defined phase diagrams are crucial for this work. The phase diagram for the lipid mixtures DSPC/DOPC/chol and DSPC/POPC/chol were previously determined (1, 2). Figure S1 shows the phase boundaries of Ld+Lo two-phase region, for DSPC/DOPC/chol and DSPC/POPC/chol. The lipid composition of samples along the trajectory used in this study are displayed by the dots.

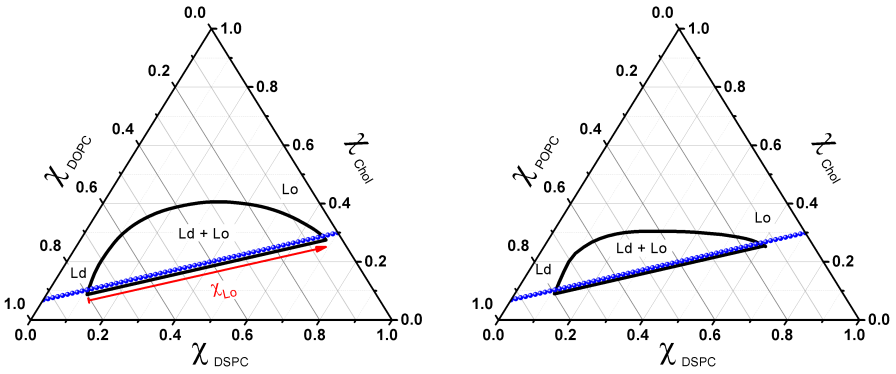

Figure S 1: Partial phase diagrams of DSPC/DOPC/chol and DSPC/POPC/chol, showing the coexistence region of Ld+Lo phases. The insert shows the fraction of Lo phase, χ_{Lo}. The dots represent the different lipid compositions of the 61 samples of the trajectory.

For bSM mixtures, bSM/DOPC/chol and bSM/POPC/chol, the phase diagrams were previously reported (2). Here, we also studied a mixture of 4-components, bSM/DOPC/POPC/chol, where the fraction of χ_{DOPC} relative to the amount of low melting lipid is given by:

$$\rho = \frac{\chi_{DOPC}}{\chi_{DOPC} + \chi_{POPC}}. \tag{1}$$

We measured the phase boundaries of bSM/DOPC/POPC /chol for $\rho = 0.4$ and $\rho = 0.75$. We interpolated the data to represent the 4-component phase diagram, Figure S2. The lipid composition used in the sample trajectories of this study are displayed by the dots, Figures S2. Similar trajectories were used for $\rho = 0.4$ and $\rho = 0.75$, using the definition of ρ in equation (1)

To calculate the fraction of Ld (χ_{Ld}) and Lo (χ_{Lo}) phases, where χ_{Ld}= 1-χ_{Lo}, we need accurate phase boundaries. The fraction of Lo phase can be determined by equation (2)

$$\chi_{Lo} = 1 - \frac{\chi_{HTm}(\chi_{Lo} = 1) - \chi_{HTm}}{\chi_{HTm}(\chi_{Lo} = 1) - \chi_{HTm}(\chi_{Lo} = 0)} \tag{2}$$

where χ_{HT_m} represents the fraction of high melting lipid, and is the independent variable along the tieline. In addition, $\chi_{HT_m}(\chi_{Lo} = 0)$ and $\chi_{HT_m}(\chi_{Lo} = 1)$ correspond to the fraction of HTm lipid in the end points of the tieline, where $\chi_{HT_m}(\chi_{Lo} = 0)$ represents the left-hand side (LHS) phase boundary, and $\chi_{HT_m}(\chi_{Lo} = 1)$ represents the right-hand side (RHS).

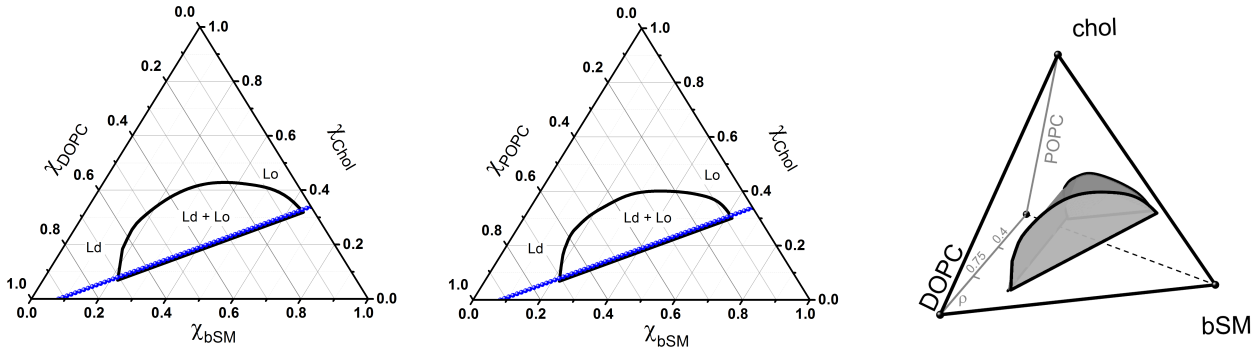

Figure S2: Partial phase diagrams of bSM/DOPC/chol and bSM/POPC/chol, showing the coexistence region of Ld+Lo phases. The dots represent the trajectory of 61 samples, for different lipid compositions. The tetrahedron shows the Ld+Lo region of 4-component lipid mixture bSM/DOPC/POPC/chol.

2 Phase boundary determination

Figure S3 shows an example of a phase boundary determination for DSPC/DOPC/chol and DSPC/POPC/chol. The phase boundary corresponds to either the intercept of linear regressions, or an abrupt change in the signal, as displayed in Figure S3 and S4. For bSM mixtures the phase boundaries and the tieline are different from the ones observed in the DSPC mixtures. Figure S4 shows the determination of the phase boundaries of bSM mixtures.

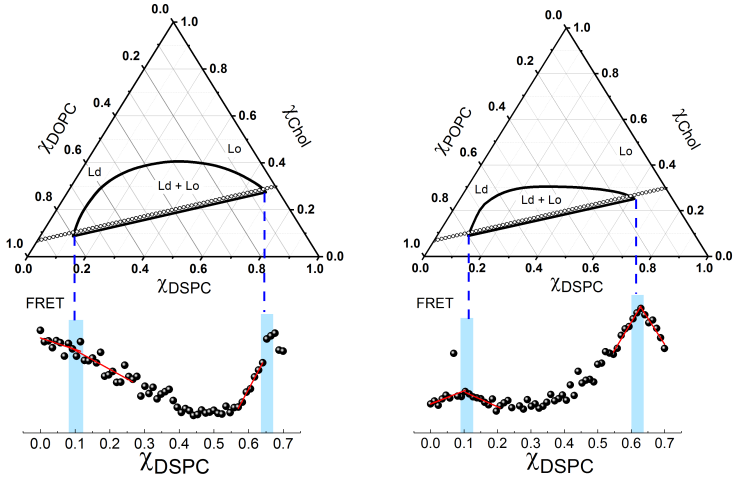

Figure S3: Example of phase boundary determination for DSPC/DOPC/chol using the FRET pair TOE and DHE, where TOE favors the Ld phase, and DHE favors the Lo phase. The errors (shadow region) were calculated from the interception of the lines plotted in each region.

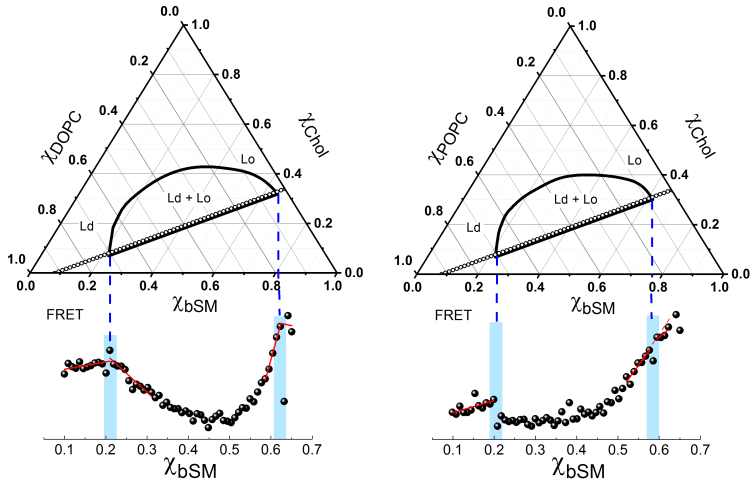

Figure S4: Example of phase boundary determination for DSPC/DOPC/chol using the FRET pair TOE and DHE, where TOE favors the Ld phase, and DHE favors the Lo phase. The errors (shadow region) were calculated from the interception of the lines plotted in each region.

The phase boundaries studied in this work agree with those that were previously reported by (Petruzielo et al. 2013; Konyakhina et al. 2013); the boundary lipid compositions are summarized in Table S1.

Lipid Composition of the phase boundaries for the tielines displayed in Figures 1 and 2

Phase Boundary	DSPC	DOPC	chol
LHS	0.11± 0.01	0.79 ± 0.01	0.10 ± 0.003
RHS	0.67± 0.01	0.06± 0.02	0.27± 0.004
Phase Boundary	DSPC	POPC	chol
LHS	0.11± 0.01	0.79 ± 0.01	0.10 ± 0.003
RHS	0.61± 0.01	0.13± 0.02	0.26± 0.004
Phase Boundary	bSM	DOPC	chol
LHS	0.22± 0.01	0.7 ± 0.01	0.08 ± 0.02
RHS	0.64± 0.01	0.03± 0.01	0.33± 0.01
Phase Boundary	bSM	POPC	chol
LHS	0.22± 0.01	0.7 ± 0.01	0.08 ± 0.02
RHS	0.61± 0.01	0.09± 0.01	0.30± 0.01

Table S1: Lipid composition of the phase boundaries for the tielines displayed in Figures 1 and 2, where the LHS phase boundary represents the boundary between Ld and Ld+Lo phase regions and the RHS phase boundary represents the boundary between Ld+Lo and Lo phase regions.

3 Single dye fluorescence

The fluorescence intensity, I, of probes that can equilibrate between two different phases, Ld and Lo, is described by the equation:

$$I = f_{Lo}\, I_{Lo} + f_{Ld}\, I_{Ld} \tag{3}$$

where f_{Ld} and f_{Lo} are the fraction of probes in the Ld and Lo phases, respectively, and I_{Ld} and I_{Lo} are the dye intensities from the Ld and Lo phases. Here, we describe the formulation that leads to equation 3.

The fraction of Ld and Lo phases changes along the tieline. Thus, the concentration of the dye in each phase depends on the lipid composition.

The fraction of Ld and Lo phases, and the fraction of dyes in each phase are described by equations (4) and (5):

$$1 = \chi_{Lo} + \chi_{Ld} \tag{4}$$

$$1 = f_{Lo} + f_{Ld} \tag{5}$$

The latter is conceptually similar to having the number of dyes found in Ld (N_{Ld}) plus the number of dyes found in Lo (N_{Lo}) equal the total amount of dye in the system (N),

$$N_{Ld} + N_{Lo} = N. \tag{6}$$

Here, we used the fraction of dyes, where equation (6) is normalized by N.

The partition coefficient is defined

$$K_p \equiv \frac{f_{Ld}/\chi_{Ld}}{f_{Lo}/\chi_{Lo}}. \tag{7}$$

According to the definition in equation (7), if

$$f_{Ld}/\chi_{Ld} > f_{Lo}/\chi_{Lo}, \quad \text{then } K_p > 1,$$

implying that $K_p > 1$ represents a partitioning that favors the Ld phase, since the dye concentration in the Ld phase is greater than the concentration in the Lo phase. On the other hand, $K_p < 1$ indicates that the dye molecule favors the Lo phase. The partition coefficient that favors the Lo phase can also be represented by $K_p' = 1/K_p$.

The intensity along the tieline, equation (3), can be written in terms of K_p and χ_{Lo}, as following. From the definition of K_p, equation 7, we can rewrite the fraction of dye in the Lo phase, f_{Lo}, using equations 4 and 5, as described below:

$$\begin{aligned} f_{Lo} &= \frac{f_{Ld}\,\chi_{Lo}}{K_p\,\chi_{Ld}} \\ f_{Lo} &= \frac{(1-f_{Lo})\,\chi_{Lo}}{K_p\,(1-\chi_{Lo})} \\ f_{Lo}[K_p(1-\chi_{Lo}) &+ \chi_{Lo}] = \chi_{Lo} \\ f_{Lo} &= \frac{\chi_{Lo}}{K_p\,(1-\chi_{Lo})+\chi_{Lo}}. \end{aligned} \tag{8}$$

From equations (8) and (5), we can rewrite f_{Ld} as:

$$\begin{aligned} f_{Ld} &= 1 - f_{Lo} \\ f_{Ld} &= 1 - \frac{\chi_{Lo}}{K_p(1-\chi_{Lo})+\chi_{Lo}} \\ f_{Ld} &= \frac{K_p(1-\chi_{Lo})}{K_p\,(1-\chi_{Lo})+\chi_{Lo}}. \end{aligned} \tag{9}$$

Replacing equations (8) and (9) in equation (3), we find,

$$I = \frac{\chi_{Lo}}{K_p\,(1-\chi_{Lo})+\chi_{Lo}}\,I_{Lo} + \frac{K_p(1-\chi_{Lo})}{K_p\,(1-\chi_{Lo})+\chi_{Lo}}\,I_{Ld}$$

$$I = \frac{\chi_{Lo}\,I_{Lo} + K_p(1-\chi_{Lo})\,I_{Ld}}{K_p\,(1-\chi_{Lo})+\chi_{Lo}} \tag{10}$$

A similar equation follows for $K_p' = 1/K_p$ (see equation 11):

$$I = \frac{K_p'\chi_{Lo}\,I_{Lo} + (1-\chi_{Lo})\,I_{Ld}}{(1-\chi_{Lo}) + K_p'\chi_{Lo}} \tag{11}$$

In this case, $K_p' > 1$ represents preference for the Lo phase, since this definition of the partition coefficient is the inverse of the definition described in equation (7).

Figure S5 shows examples of intensity profiles along the tieline, where the fraction of phases are represented by χ_{Lo}. In this example, we fixed the values of I_{Ld} and I_{Lo}, assuming $I_{Ld} = 3I_{Lo}$. Intensity along the trajectory calculated for different values of K_p.

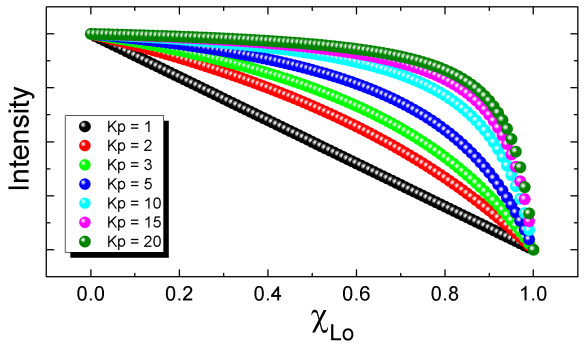

Figure S 5: Theoretical Intensity along a thermodynamic tieline of fluorescent dyes that equilibrate between two phases. Equation 11 is plotted using different partition coefficients and fixed values of I_{Ld} and I_{Lo}, where $I_{Ld} = 3\, I_{Lo}$.

3.1 Quenching Correction

Since self-quenching of the fluorescence signal would distort the analyses of single dye fluorescence or FRET, we have previously studied the ideal dye concentration to use in our experiments. Figure S6 shows the fluorescence emission of Bodipy-PC and TOE, measured in the end-points of the tieline for DSCP/DOPC/chol, DSCP/POPC/chol, bSM/POPC/chol and bSM/DOPC/chol, as a function of the dye/lipid ratio.

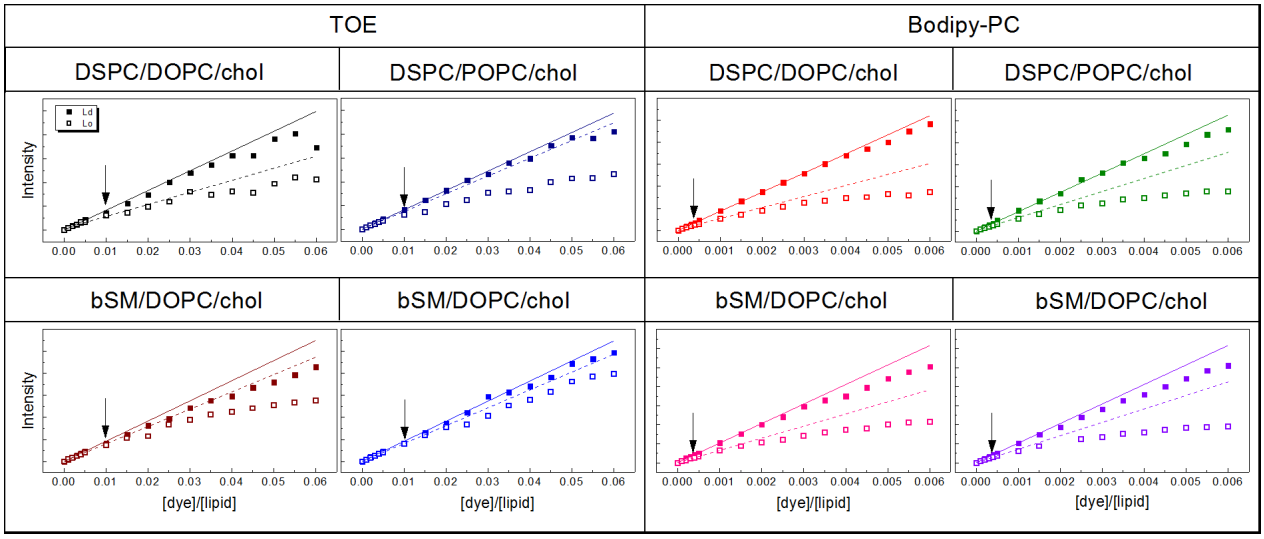

Figure S 6: Self-quenching effect of TOE and Bodipy-PC observed in the Ld phase (solid square) and the Lo phase (open square). Intensities of TOE and Bodipy-PC within increasing dye concentration were measured in the end points of the tieline ($\chi_{Lo} = 0$, Ld phase) and ($\chi_{Lo} = 1$, Lo phase). The deviation from the linear behavior indicates fluorescence self-quenching. Solid line represents a fit of the linear part of the data for Ld phase, and the dashed line for the Lo phase. For single dye and FRET experiments we used [dye]/[lipid]= 0.01 for TOE, and [dye]/[lipid]=0.0004 for Bodipy-PC. Arrows show the [dye]/[lipid] used in the experiments.

As displayed in Figure S6, the line shown in the graphs represent infinite dilution. Deviation from this line indicates self-quenching. We used a dye concentration where negligible quenching effects were observed. The dye/lipid ratio used in this work for each lipid mixture is indicated in the legend of Figure S6.

In addition, the concentration of the dye in each phase changes within the changing phase fractions along the tieline. Given K_p, the concentration of the dye in each phase can be calculated for each point of the tieline. Using the above information, which relates the dye concentration to a certain percentage of fluorescence self-quenching, we can also correct for self-quenching effects.

4 FRET

The sensitized acceptor emission, here termed as FRET, of probes that equilibrate between two different phases, Ld and Lo, is given by equation (12), as previously reported by (3):

$$FRET = F_{Ld}\ \frac{f^A_{Ld}\ f^D_{Ld}}{\chi_{Ld}} + F_{Ld}\ \frac{f^A_{Lo}\ f^D_{Lo}}{\chi_{Lo}}, \tag{12}$$

where F_{Ld} and F_{Lo} are the FRET signals from the Ld and Lo phases, respectively. The fraction of probes in the Ld and Lo phases are given by f_{Ld} and f_{Lo}, as described above; the indices A and D refer to acceptor and donor, respectively.

As similarly described in equation (5), the fraction of probes in the Ld or in the Lo phases are constrained by the total amount of probe:

$$1 = f^A_{Ld} + f^A_{Lo} \tag{13}$$

$$1 = f^D_{Ld} + f^D_{Lo} \tag{14}$$

Using the definition of the partition coefficient, equation (7), we can write f_{Lo} and f_{Ld} as functions of K_p and the fraction of the Lo phase, χ_{Lo}, as we described in equations 8 and 9:

$$f^A_{Lo} = \frac{\chi_{Lo}}{K^A_p\,(1-\chi_{Lo}) + \chi_{Lo}} \tag{15}$$

$$f^D_{Lo} = \frac{\chi_{Lo}}{K^D_p\,(1-\chi_{Lo}) + \chi_{Lo}}, \tag{16}$$

$$f^A_{Ld} = \frac{K^A_p(1-\chi_{Lo})}{K^A_p\,(1-\chi_{Lo}) + \chi_{Lo}} \tag{17}$$

$$f^D_{Ld} = \frac{K^D_p(1-\chi_{Lo})}{K^D_p\,(1-\chi_{Lo}) + \chi_{Lo}}. \tag{18}$$

Using the definitions of f_{Lo} and f_{Ld} described in equations 16 and 18:

$$\frac{f_{Ld}^A f_{Ld}^D}{\chi_{Ld}} = \frac{1}{(1-\chi_{Lo})}\left\{\frac{K_p^A(1-\chi_{Lo})}{[K_p^A\,(1-\chi_{Lo})+\chi_{Lo}]}\frac{K_p^D(1-\chi_{Lo})}{[K_p^D\,(1-\chi_{Lo})+\chi_{Lo}]}\right\} \tag{19}$$

$$\frac{f_{Ld}^A f_{Ld}^D}{\chi_{Ld}} = \frac{K_p^A\,K_p^D\,(1-\chi_{Lo})}{[K_p^A\,(1-\chi_{Lo})+\chi_{Lo}]\,[K_p^D\,(1-\chi_{Lo})+\chi_{Lo}]}, \tag{20}$$

$$\frac{f_{Lo}^A f_{Lo}^D}{\chi_{Lo}} = \frac{1}{\chi_{Lo}}\left\{\frac{\chi_{Lo}}{[K_p^A\,(1-\chi_{Lo})+\chi_{Lo}]}\frac{\chi_{Lo}}{[K_p^D\,(1-\chi_{Lo})+\chi_{Lo}]}\right\} \tag{21}$$

$$\frac{f_{Lo}^A f_{Lo}^D}{\chi_{Lo}} = \frac{\chi_{Lo}}{[K_p^A\,(1-\chi_{Lo})+\chi_{Lo}]\,[K_p^D\,(1-\chi_{Lo})+\chi_{Lo}]}. \tag{22}$$

Therefore, the sensitized acceptor emission, FRET, can be rewritten using equations (20) and (22) in equation (12). The following equation is an analytical solution for FRET that depends on known or measurable parameters, such as the FRET signal in the phase boundaries, F_{Ld} and F_{Lo}, the fraction of phases (according to the Lever Arm rule), and the parameters to be fitted, such as the partition coefficient of the probes, K_p^A and K_p^D,

$$FRET = \frac{F_{Ld}\,K_p^A\,K_p^D(1-\chi_{Lo})+F_{Lo}\,\chi_{Lo}}{[K_p^A\;+\;(1-K_p^A)\chi_{Lo}]\,[K_p^D\;+\;(1-K_p^D)\chi_{Lo}]}. \tag{23}$$

Figure S7 shows examples of FRET profiles along the tieline, using equation (23). We considered the dyes of the FRET pair partition into different phases (left graph), and both partitioning into the Ld phase. For illustration, we fixed the acceptor K_p and plotted the FRET profiles for different K_p values of the donor.

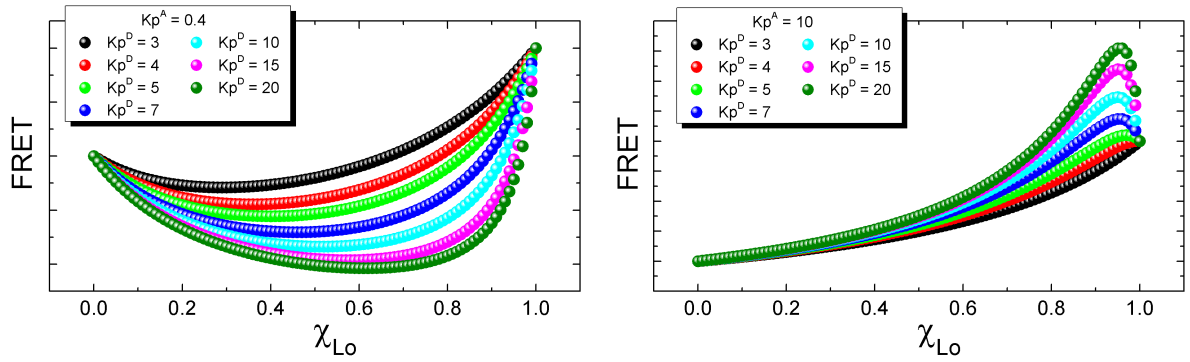

Figure S 7: Theoretical FRET along a thermodynamic tieline of fluorescent dyes that equilibrate between two phases. Equation 23 is plotted using different partition coefficients and fixed values of F_{Ld} and F_{Lo}. Left, acceptors favor the Lo phase, $K_p = 0.4$, and $I_{Lo} = 1.5\,I_{Ld}$. Right, acceptors favor the Ld phase, $K_p = 10$, and $I_{Lo} = 3\,I_{Ld}$.

Equation (23) was developed using the definition of K_p described in equation (7), where $K_p > 1$

indicates that the probe favors the Ld phase. Using the inverse definition, $K'_p = 1/K_p$, where $K'_p > 1$ indicates a preference for the Lo phase, FRET can be written as equation (24):

$$FRET = \frac{F_{Ld} + \chi_{Lo}\left(F_{Lo}\, K_p'^{A}\, K_p'^{D} - F_{Ld}\right)}{\left[1 + (K_p'^{A} - 1)\chi_{Lo})\right]\left[1 + (K_p'^{D} - 1)\chi_{Lo})\right]}. \tag{24}$$

As an exercise, the readers can replace $1/K'_p$ in equation 23, in order to obtain equation 24.

4.1 Partition coefficient of DHE

The partition coefficient of cholesterol can be obtained from the phase diagram, wit. As an example, we describe the partition coefficient of cholesterol in the DSPC/DOPC/chol mixture. The fraction of cholesterol in the Ld phase, (LHS) phase boundary ($\chi_{Lo} = 0, \chi_{Ld} = 1$), corresponds to $f_{Ld} = 0.10$. The fraction of cholesterol in the Lo phase, (RHS) phase boundary ($\chi_{Lo} = 1$), corresponds to $f_{Lo} = 0.27$. Therefore:

$$K_p = \frac{0.10}{0.27} = \frac{1}{2.7} = 0.37\ . \tag{25}$$

Since DHE is a very close cholesterol analogue, we assume DHE partitions between Ld and Lo phases in the same way as cholesterol. Table S2 shows the partition coefficient of cholesterol or DHE for all lipid mixtures used in this work, where K_p (Ld) follows the definition described in equation 7, and K'_p (Lo) means $K_p > 1$ favors the Lo phase.

DHE partition coefficient		
Lipid mixture	K_p (Ld)	K'_p (Lo)
DSPC/DOPC/chol	0.37 ± 0.01	2.7 ± 0.1
DSPC/POPC/chol	0.39 ± 0.01	2.5 ± 0.1
bSM/DOPC/chol	0.25 ± 0.01	4.0 ± 0.1
bSM/DOPC/chol	0.27 ± 0.01	3.8 ± 0.1

Table S2: Partition coefficient of DHE obtained from the phase diagrams.

5 Data collection of the fluorescence emission

The fluorescence emission of the single-dye experiments or the FRET signal were collected using the excitation and emission wavelengths described in Table S3. It should be noted that for FRET experiments we excite the donor, and monitor the fluorescence emission of the acceptor (sensitized acceptor emission). Moreover, we also monitored the light scattering for each sample at $\lambda = 400$ nm, without dye excitation.

Wavelengths monitored in the Fluorescence studies

Single dye fluorescence		
Dye	λ_{ex} (nm)	λ_{em} (nm)
TOE	284	335
Bodipy-PC	500	520
FRET experiments: fluorescence emission		
Dye	λ_{ex} (nm)	λ_{em} (nm)
TOE	284	335
DHE	327	393
Bodipy-PC	500	520
FRET experiments: acceptor fluorescence excited by the donor		
Pair	λ_{ex} (nm)	λ_{em} (nm)
TOE/DHE	284	393
DHE/Bodipy-PC	327	520
TOE/Bodipy-PC	284	520

Table S3: Excitation and emission wavelengths monitored in single dye and FRET experiments.

As previously reported (3 - 5), the acceptor fluorescence emission excited by the donor needs to be corrected for any signal that is not related to FRET. Because of that, we also monitored the fluorescence emission of each dye in the FRET experiments. Controls and blanks are also required in these experiments in order to obtain sensitized acceptor emission (FRET) as previously described in (3 - 5).

Figure S8 shows examples of the fluorescence signal collected in the single dye experiments, for lipid mixtures that form macro- and nanodomains, Figure S8 A and B. We compare these signals to the light scattering obtained for each sample. Similar comparisons are shown in Figure S8 C and D, for the FRET experiments. As shown in Figure S8, the fluorescence signal exceeds that of the light scattering by about 10 to 100-fold.

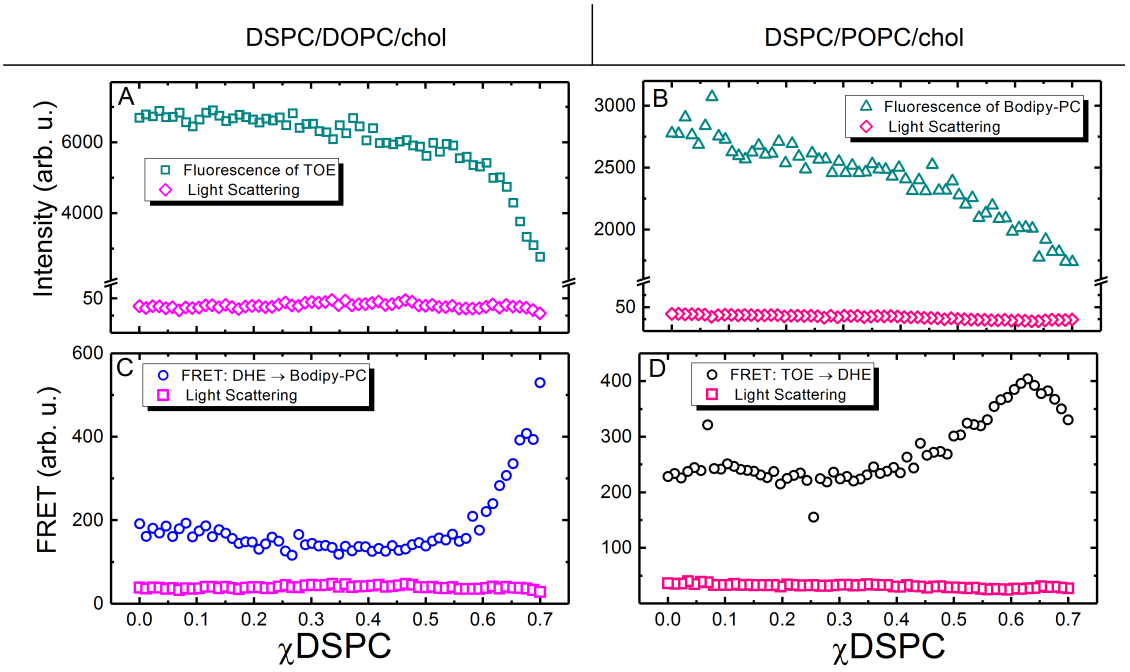

Figure S8: Comparison between the fluorescence emission measured on single dye experiments and the light scattering for different lipid compositions along the tieline: (A) for DSPC/DOPC/chol, mixtures that forms macrodomains, (B) DSPC/POPC/chol, mixture that forms nanodomains. Comparison between the FRET signal and the light scattering for different lipid compositions along the tieline: (C) for DSPC/DOPC/chol and (D) for DSPC/POPC/chol.

6 FRET simulations

6.1 Parametrization

The simulations use a list of parameters that take into account the structural properties of the lipid bilayer, such as the area occupied by the Ld and the Lo phases, and the thickness of each phase. In addition, each FRET pair is described by a set of specific parameters, as their position in the bilayer and the Forster distance, R_0. Tables S4 and S5 list the parametrization used in the Monte Carlo simulations.

6.2 Validation

For macrocoscopic phase separation, the number of dyes in the domain interface is negligible compared to the amount of dyes distributed in the macrodomain or in the surrounding phase. Reproducing this model using Monte Carlo (MC) simulations, we are able to compare the simulated FRET with the analytical solution described by Buboltz (3). Figure S9 shows FRET profiles along a thermodynamic tieline calculated using MC simulations, for different partition coefficients (dots), and the FRET profiles calculated from equation 9 (line). The comparison between MC simulations and the analytical solution

Parameters used in the Monte Carlo simulations

Parameter	Ld value	Lo value
Bilayer structural parameters		
Headgroup thickness (Å)	4.75	6.1
Hydrocarbon thickness (Å)	29.0	37.6
Area per lipid (Å^2)	63.1	43.2
TOE parameters		
Monolayer location [(Å) from bilayer center]	10.5	10.5
Monolayer location distribution width (Å)	2	2
DHE parameters		
Monolayer location [(Å) from bilayer center]	9.5	13.8
Monolayer location distribution width (Å)	2	2
Bodipy-PC parameters		
Monolayer location [(Å) from bilayer center]	11.5	13.8
Monolayer location distribution width (Å)	2	2

Table S4: Parameters used in the Monte Carlo simulations for Ld and Lo phases.

Parameters used in the Monte Carlo simulations

Fixed parameters	
Number of donors for averaging	10^4
Exclusion radius per probe (Å^2)	5
Probe concentration (mole fraction)	
TOE	0.01
DHE	0.01
Bodipy-PC	0.0004
Energy transfer parameters	
R_0 (TOE $\rightarrow$ DHE) (Å)	24
R_0 (DHE $\rightarrow$ Bodipy-PC) (Å)	28
R_0 (TOE $\rightarrow$ Bodipy-PC) (Å)	25

Table S5: Parameters used in the Monte Carlo simulations related to FRET

shows a good agreement, thus validating our code.

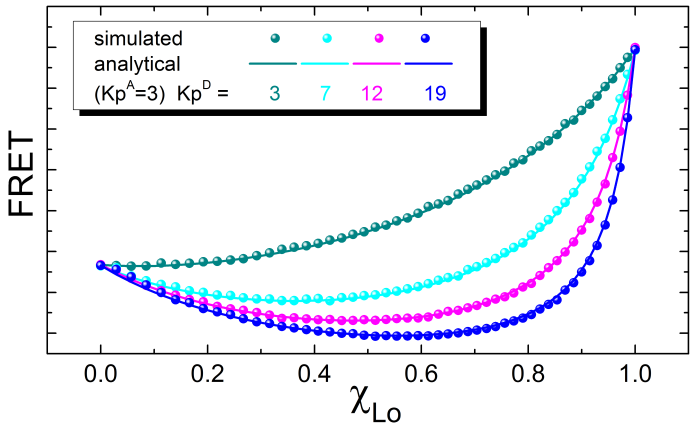

Figure S9: Comparison between the FRET calculated using Monte Carlo simulations and the analytical solution, equation 23. The partition coefficient of the acceptor is fixed, $K_p^A = 3$ and different donor partition coefficients were tested, $K_p^D = 3$, 7, 12 and 19. The decrease of K_p reduces the valley-shape in the FRET profiles.

6.3 Influence of domain size in FRET curves

Using Monte Carlo simulations, we tested the influence of the domain size on FRET curves. Figure S10 shows the simulated FRET considering different domain sizes, represented by the domain radius, R_d. Decreasing the domains sizes leads to similar effects on the FRET profiles as decreasing the partition coefficient, as shown in Figure S10.

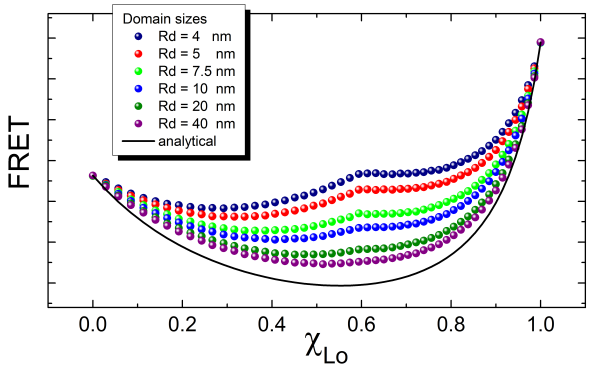

Figure S10: Influence of domain size in FRET profiles. The analytical solution, equation, represents the size of macrodomains. The decrease of the domain size reduces the valley-shape in the FRET profiles.

We have tested to fit our experimental data with 3 free parameters the partition coefficient of donor and acceptor, and the domain size. These analyses frequently result in 2 possible solutions: higher values of K_p leading to a small domain size or lower values of K_p leading to a large domain size. In order to avoid any misinterpretation in our analysis, we measure the K_p using single dye fluorescence, a completely independent experiment, and then we focus in the investigation of the domain size.

7 Partition coefficient measured on GUVs

We measured the partition coefficient of Bodipy-PC on giant unilamellar vesicles (GUVs) using line scans, as described in the main text. We observed that the Ld phase is brighter than the Lo phase, not only because Bodipy-PC prefers Ld, but also because the fluorescence of Bodipy-PC is intrinsically brighter in the Ld phase, compared to the same amount of dye in the Lo phase. Therefore, we applied a correction related to the quantum yield of the dye in each phase.

In addition to that, we noticed that the intensity of Ld and Lo depends on the fractions of the phases, and the Kp measured by single dye fluorescence (or FRET) takes into account the total intensity from the Ld and the total intensity from the Lo phase. Therefore, we calculated the intensity from Ld and from Lo, considering Ld and Lo surface areas on the GUV. We observed similar intensity values for 10 different line scans, in each phase, suggesting a homogeneous distribution of the dye in each phase (Figure 2, main text). Therefore, I_{Ld}^{GUV} and I_{Lo}^{GUV} can be assumed constant along Ld or Lo surface areas. Thus, the total intensity from Ld or Lo phases, I_{Ld}^{T} and I_{Lo}^{T}, are given by:

$$I_{Ld}^{T} = \int_{S^{Ld}} I_{Ld}^{GUV} da = I_{Ld}^{GUV} \int_{S^{Ld}} da = I_{Ld}^{GUV} S_{Ld} \tag{26}$$

$$I_{Lo}^{T} = \int_{S^{Lo}} I_{Lo}^{GUV} da = I_{Lo}^{GUV} \int_{S^{Lo}} da = I_{Ld}^{GUV} S_{Lo} \tag{27}$$

where S_{Ld} and S_{Lo} represent the surface areas of each phase.

Then, to measure the Kp, we compare the intensities from Ld and Lo phases, corrected by the quantum yield of each phase, as described in equation 28:

$$K_p = \frac{I_{Ld}^{GUV}\, S_{Ld}/\Phi_{Ld}}{I_{Lo}^{GUV}\, S_{Lo}/\Phi_{Ld}} = \frac{I_{Ld}^{GUV}\, S_{Ld}}{I_{Lo}^{GUV}\, S_{Lo}} \frac{\Phi_{Lo}}{\Phi_{Ld}} \tag{28}$$

where the ratio $\frac{S^{Ld}}{S^{Lo}}$ is related to the mole fraction of each phase, except that the Ld phase occupies about 30% more area than the Lo phase. For our experiments, GUVs were prepared with the same mole fraction of Ld and Lo phases, then $\frac{S^{Ld}}{S^{Lo}} \approx 1.3$.

8 Domain sizes on GUVs

GUVs were prepared using the electroformation procedure (6). For partition coefficient measurements, the lipid films were hydrated and swelled in a sucrose solution 100 mM at 55^oC, then cooled to room temperature (23^oC) at a temperature rate of 2^oC/hour. For domain size observations along a thermodynamic tieline, GUVs were cooled at a slower rate of 0.8^oC/hour. Figure S11 shows GUVs with different sizes. Figure S11 (left) displays a GUV of diameter, $D_v = 32$ μm, and (right) with $D_v = 19$

μm. The area fraction of the domain in these GUVs are similar, although the size of the domains are different. Intuitively, the largest GUV has a large domain size, $R_d \approx 16 \pm 1$ μm.

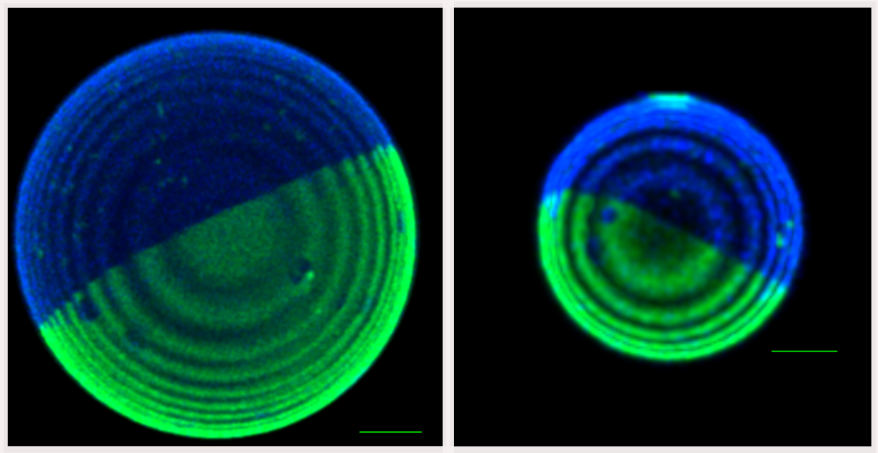

Figure S11: GUV of bSM/DOPC/chol = 0.44/0.35/0.21, displaying the coexistence of Ld (green) and Lo phases (blue). Left, bigger GUV with diameter of 32 μm and domain size of radius $R_d \approx 16$ μm. Right, smaller GUV with diameter of 19 μm and domain size of radius $R_d \approx 9.5$ μm. Both GUVs have similar domain area fractions, $\approx 45\%$ of the GUV area.

9 Nanodomain size does not depend on vesicle size, SANS

Our analysis shows that the domain sizes of nanodomains do not depend on the vesicle size. We previously reported the size of nanodomains measured by SANS (7), for DSPC/POPC/chol, where vesicles of different sizes, Rv = 30, 50, 100 and 200 nm, were prepared using a mini-extruder (Avanti Polar Lipids, Alabaster, AL, USA). Figure S12 shows the sizes of nanodomains of DSPC/POPC/chol for different vesicle sizes.

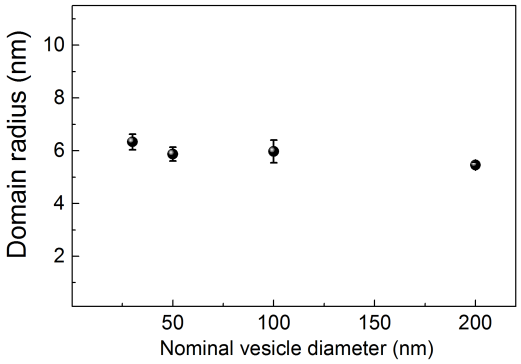

Figure S12: The size of nanodomains measured by SANS for vesicles with different sizes, R_v = 30, 50, 100 and 200 nm. The size of domains in the nanoscopic regime seems to be independent of the vesicle sizes.

Details about liposome preparation and SANS measurements can be found at (7, 8).

10 References

1. Konyakhina, T.M., J. Wu, J.D. Mastroianni, F. A. Heberle, and G.W. Feigenson. 2013. Phase diagram of a 4-component lipid mixture: DSPC/DOPC/POPC/chol. Biochim. Biophys. Acta - Biomembr. 1828: 2204 - 2214.

2. Petruzielo, R.S., F. A. Heberle, P. Drazba, J. Katsaras, and G.W. Feigenson. 2013. Phase behavior and domain size in sphingomyelin-containing lipid bilayers. Biochim. Biophys. Acta. 1828: 1302?1313.

3. Buboltz, J.T. 2007. Steady-state probe-partitioning fluorescence resonance energy transfer: A simple and robust tool for the study of membrane phase behavior. Phys. Rev. E - Stat. Nonlinear, Soft Matter Phys. 76: 1 - 7.

4. Heberle, F. A., J.T. Buboltz, D. Stringer, and G.W. Feigenson. 2005. Fluorescence methods to detect phase boundaries in lipid bilayer mixtures. Biochim. Biophys. Acta - Mol. Cell Res. 1746: 186 - 192.

5. Heberle, F.A., J. Wu, S.L. Goh, R.S. Petruzielo, and G.W. Feigenson. 2010. Comparison of Three Ternary Lipid Bilayer Mixtures: FRET and ESR Reveal Nanodomains. Biophys. J. 99: 3309 - 3318.

6. Angelova, M.I., and D.S. Dimitrov. 1986. Liposome electroformation. Faraday Discuss. Chem. Soc. 81: 303.

7. Usery, R.D., T.A Enoki, S.P.P. Wickramasinghe, M.D. Weiner, W.C. Tsai, M.B. Kim, S. Wang, T.L.L. Torng, D.G Ackerman, F.A. Heberle, J. Katsaras, and G.W. Feigenson. 2017. Line Tension Controls Liquid-Disordered+ Liquid-Ordered Domain Size Transition in Lipid Bilayers. Biophys. J. 112: 1431 - 1443.

8. Heberle, F.A., R.S. Petruzielo, J. Pan, P. Drazba, N. Kucerka, R.F. Standaert, G.W. Feigenson, and J. Katsaras. 2013. Bilayer thickness mismatch controls domain size in model membranes. J. Am. Chem. Soc. 135: 6853 - 6859.